Structural Engineering and Mechanics, *Vol. 61, No. 2 (2017) 255-266*
DOI: https://doi.org/10.12989/sem.2017.61.2.255

Curvilinear free-edge form effect on stability of perforated laminated composite plates

Zihni Zerin[a], Muhammed Fatih Başoğlu[*] and Ferruh Turan[b]

Department of Civil Engineering, Ondokuz Mayis University, Samsun 55139, Turkey

(Received June 15, 2016, Revised October 18, 2016, Accepted November 6, 2016)

Abstract. In this study, self-supporting roofing elements especially convenient for large-span structures such as stadium, airport terminal, mall, coliseum, etc. were examined with respect to critical buckling load. These elements were assumed as laminated composite plates and, variation of free-edge forms, cutout types and lamination configurations were used as design parameters. Based on the architectural feature and structural requirements, the effects of curvilinear free-edge form on critical buckling load were focused on in this research. Within this scope, 14 types of lamination configuration were specified according to various orientation angle, number and thickness of plies with a constant value of total plate thickness. Besides that, 6 different types of cutout and 3 different free-edge forms were determined. By combining all these parameters 294 different critical buckling load analyses were performed by using ANSYS Mechanical software based on finite element method. Effects of those parameters on critical buckling load were evaluated referring to the obtained results. According to the results presented here, it may be concluded that lamination conditions have more significant influence on the critical buckling load values than the other parameters. On the other hand, it is perceived that curvilinear free-edge forms explicitly undergo changings depending on lamination conditions. For future work, existence of delamination might be considered and progression of the defect could be investigated by using non-linear analysis.

Keywords: laminated composite plate; self-supporting; curvilinear free-edge; plate with cutout, finite element method; stability

1. Introduction

Roofing systems of structures such as stadium, airport terminal, mall, coliseum, etc. require high technical and design specifications for the individual elements and the entire roof system because of their large-span feature (Carpinteri *et al.* 2016, Islam *et al.* 2005). Thereupon, the necessity of cutout and non-linear edge form in these elements are typically demanded by practical concern and architectural restrictions. For instance, cutouts in plate elements are needed for skylight openings and rainwater piping systems. In such cases, the existence of these factors change the stress concentrations in the plates and may reduce their stability. The buckling of such plates has received the attention of many researchers over several decades (Ghannadpour *et al.* 2006, Guo *et al.* 2008, Yazici 2009, Al-Qablan *et al.* 2009, Yazici *et al.* 2003, Baba 2007, Baba and Baltaci 2007, Al-Jameel and Albazzaz 2014, Narayana *et al.* 2014, Kumar and Singh 2010, Jadhav and Chavan 2013, Baltacı *et al.* 2006, Joshi *et al.* 2013, Yazdani *et al.* 2013).

It was reported that in some experimental and/or numerical solutions for the buckling of perforated square/rectangular plates subjected to uniaxial compression or shear loading, in the fiber orientations one which agglomerate in the direction of load represents higher buckling load than the one agglomerate perpendicular to the load direction (Ghannadpour *et al.* 2006, Guo *et al.* 2008, Yazici 2009). In addition, if the aspect ratio of the cutout is equal to 1 any considerable difference would not be observed in cutouts between with rounded corner and cutting corner.

In the work, Finite Element Method (FEM) was used to study the buckling of perforated square/rectangular plates subjected to shear loading, biaxial and/or uniaxial compression, it was found that the reduction of the buckling load by virtue of an increase in the cutout size is distinct in the case of shear loading as compared to uniaxial and biaxial compression (Al-Qablan *et al.* 2009, Yazici *et al.* 2003, Al-Qablan *et al.* 2010). Under the uniaxial compression cases, the cutout size had a more obvious effect on some of the fiber orientation angles which was less obvious on others.

The investigations used the finite element and experimental or analytical methods to search the buckling of rectangular plates subjected to in-plane compressive loading illustrated that the buckling loads of the plates with anti-symmetric layup were higher as compared to symmetric ones (Baba 2007, Baba and Baltaci 2007, Ö zben 2009).

The findings of numerical studies by the finite element method to determine the effects of cutout orientation on the

∗Corresponding author, Ph.D. Student
E-mail: fatih.basoglu@omu.edu.tr
[a]Associate Professor
[b]Ph.D. Student

ISSN: 1225-4568 (Print), 1598-6217 (Online)

Fig. 1 Landesgartenschau Exhibition Hall, Stuttgart, Germany (Nebelsick and Halbe 2014)

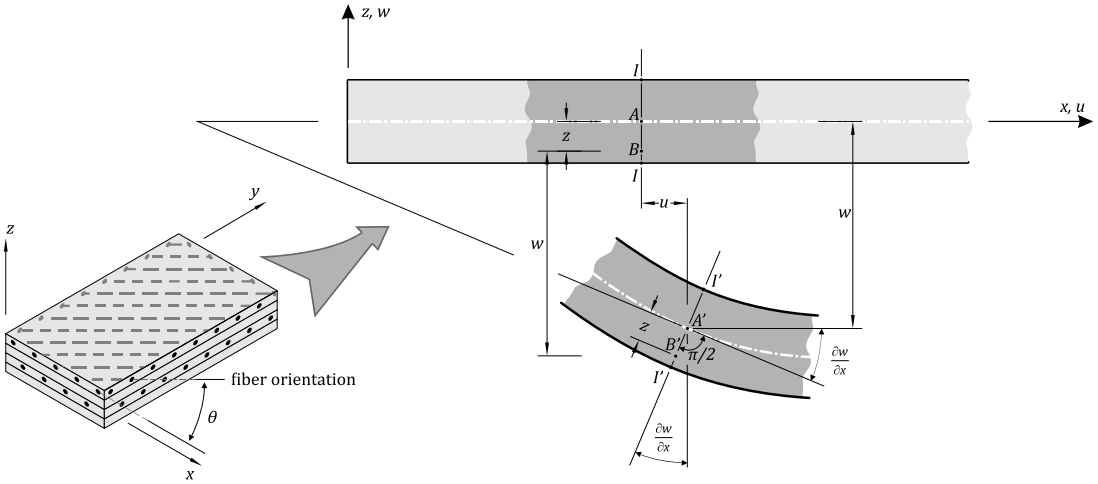

Fig. 2 The Kirchhoff-Love hypothesis for bending of thin laminates (Ochoa and Reddy 1992)

buckling behavior of laminated composite plates showed that in the orientation of the cutout's major axis/side one which is parallel to the loading direction exhibits higher buckling load than the one perpendicular to the load direction (Ghannadpour *et al.* 2006, Al-Jameel and Albazzaz 2014, Narayana *et al.* 2014, Kumar and Singh 2010).

The above studies dealt with buckling behavior of composite plates depend on various layup, fiber orientation, perforation shape and loading condition parameters by using FEM. Also there appeared many other investigations about stability analysis of laminated composite plates in literature (Shukla *et al.* 2005, Singh and Chakrabarti 2012, Jadhav and Chavan 2013, Thai and Choi 2014, Reddy *et al.* 2010, Yazdani *et al.* 2013, Zhong and Gu 2007, Zerin *et al.* 2016, Baltaci *et al.* 2007, Civalek 2009, Civalek 2008, Rezaiee-Pajand *et al.* 2012). However, the studies with both the cutout shape and the lamination configuration parameters accompanied by the curvilinear edged form are more limited and further investigations are necessary.

A self-supporting featured roofing concept not only protecting the building and its occupants from the effects of weather but also not requiring a load-bearing system is assumed in this paper. One is especially convenient to cover large-span structures and to actualize distinctive architectural ideas such as in Fig. 1 (Nebelsick and Halbe 2014). Meanwhile, some restrictions may require for composite plate elements of this concept used as design parameters such as curvilinear free-edge forms, various cutout shapes with/out rounded corner and diverse lamination configurations were determined. Due to the self-supporting feature, the elements of this kind of roofing structures could be able to bear with in-plane compressive loads. Therefore, it is focused on investigating the effects of the parameters on stability of these plate elements by using Finite Element Method (FEM). It is aimed that a valuable contribution to the literature could be made by pointing out the effect of the curvilinear free-edge forms on critical buckling load of laminated composite plates.

2. Theory and formulations

2.1 Strain-displacement relations

The laminate coordinate system is defined as the xy-plane coinciding with the mid-plane of the laminate (Ochoa and Reddy 1992, Reddy 2004). The geometry is illustrated in Fig. 2. At a point (x, y, z) in the un-deformed laminate, the displacements u, v, w are written as

$$u(x,y,z,t) = u_0(x,y,t) + z \cdot \phi_x(x,y,t)$$
$$v(x,y,z,t) = v_0(x,y,t) + z \cdot \phi_y(x,y,t) \quad (1)$$
$$w(x,y,z,t) = w_0(x,y,t)$$

where u_0, v_0, w_0 are the displacements on the xy-plane and ϕ_x, ϕ_y are the rotations of the transverse normal in the xz- and yz-planes, and equal to $-\partial w_0/\partial x$ and $-\partial w_0/\partial y$, respectively (Ochoa and Reddy 1992, Reddy 2004). Also t denotes time.

The laminate strains are of general form

$$\begin{Bmatrix}\varepsilon_{xx}\\ \varepsilon_{yy}\\ \varepsilon_{xy}\end{Bmatrix}=\begin{Bmatrix}\varepsilon_{xx}^{(0)}\\ \varepsilon_{yy}^{(0)}\\ \varepsilon_{xy}^{(0)}\end{Bmatrix}+z\begin{Bmatrix}\varepsilon_{xx}^{(1)}\\ \varepsilon_{yy}^{(1)}\\ \varepsilon_{xy}^{(1)}\end{Bmatrix} \tag{2}$$

where $\left(\varepsilon_{xx}^{(0)},\varepsilon_{yy}^{(0)},\varepsilon_{xy}^{(0)}\right)$ and $\left(\varepsilon_{xx}^{(1)},\varepsilon_{yy}^{(1)},\varepsilon_{xy}^{(1)}\right)$ represent mid-plane and bending strain vectors, respectively (Baltacı *et al.* 2006, Reddy 2004), and are given by

$$\begin{Bmatrix}\varepsilon_{xx}\\ \varepsilon_{yy}\\ \varepsilon_{xy}\end{Bmatrix}=\begin{Bmatrix}\dfrac{\partial u_0}{\partial x}+\dfrac{1}{2}\left(\dfrac{\partial w_0}{\partial x}\right)^2\\ \dfrac{\partial v_0}{\partial y}+\dfrac{1}{2}\left(\dfrac{\partial w_0}{\partial y}\right)^2\\ \dfrac{\partial u_0}{\partial y}+\dfrac{\partial v_0}{\partial x}+\dfrac{\partial w_0}{\partial x}\cdot\dfrac{\partial w_0}{\partial y}\end{Bmatrix}+z\begin{Bmatrix}-\dfrac{\partial^2 w_0}{\partial x^2}\\ -\dfrac{\partial^2 w_0}{\partial y^2}\\ -2\dfrac{\partial^2 w_0}{\partial x\partial y}\end{Bmatrix} \tag{3}$$

2.2 Constitutive relations

The force and moment resultants $(\{\boldsymbol{N}\},\{\boldsymbol{M}\})$ can be expressed in terms of mid-plane and bending strain vectors $(\{\boldsymbol{\varepsilon^0}\},\{\boldsymbol{\varepsilon^1}\})$ through the laminate constitutive equations as below

$$\begin{Bmatrix}\{\boldsymbol{N}\}\\ \{\boldsymbol{M}\}\end{Bmatrix}=\begin{bmatrix}[\boldsymbol{A}] & [\boldsymbol{B}]\\ [\boldsymbol{B}] & [\boldsymbol{D}]\end{bmatrix}\cdot\begin{Bmatrix}\{\boldsymbol{\varepsilon^0}\}\\ \{\boldsymbol{\varepsilon^1}\}\end{Bmatrix} \tag{4}$$

where $[\boldsymbol{A}]$, $[\boldsymbol{D}]$ and $[\boldsymbol{B}]$ show the stiffnesses of extensional, bending, and bending-extensional coupling of a laminate, respectively (Baltacı *et al.* 2006, Reddy 2004).

2.3 Equations of motion

By using the principle of virtual displacements the equations of motion can be yielded in the form

$$\begin{aligned}\frac{\partial N_{xx}}{\partial x}+\frac{\partial N_{xy}}{\partial y}&=I_o.\ddot{u}-I_1.\frac{\partial\ddot{w}}{\partial x}\\ \frac{\partial N_{xy}}{\partial x}+\frac{\partial N_{yy}}{\partial y}&=I_o.\ddot{v}-I_1.\frac{\partial\ddot{w}}{\partial y}\\ \frac{\partial^2 M_{xx}}{\partial x^2}+2\frac{\partial^2 M_{xy}}{\partial y\partial x}+\frac{\partial^2 M_{yy}}{\partial y^2}+N(w)+q&=I_o.\ddot{w}+I_2.\left(\frac{\partial^2\ddot{w}}{\partial x^2}+\frac{\partial^2\ddot{w}}{\partial y^2}\right)\\ &\quad+I_1.\left(\frac{\partial\ddot{u}}{\partial x}+\frac{\partial\ddot{v}}{\partial y}\right)\end{aligned} \tag{5}$$

where $\left(N_{xx},N_{yy},N_{xy}\right)$ and $\left(M_{xx},M_{yy},M_{xy}\right)$ are force and moment resultants (Fig. 3) and $N(w)$ is nonlinear expression (Ochoa and Reddy 1992, Reddy 2004, Shukla *et al.* 2005).

$$\begin{aligned}N(w)=&\frac{\partial}{\partial x}\left(N_{xx}\frac{\partial w}{\partial x}+N_{xy}\frac{\partial w}{\partial y}\right)\\ &+\frac{\partial}{\partial y}\left(N_{xy}\frac{\partial w}{\partial x}+N_{yy}\frac{\partial w}{\partial y}\right)\end{aligned} \tag{6}$$

2.4 Finite element model

2.4.1 Weak form

Multiply the equations in Eq. (5) with relevant weight functions $(\delta u,\delta v,\delta w)$ and integrate over the element domain Ω^e (Ochoa and Reddy 1992). Hence, weak forms are obtained in the form

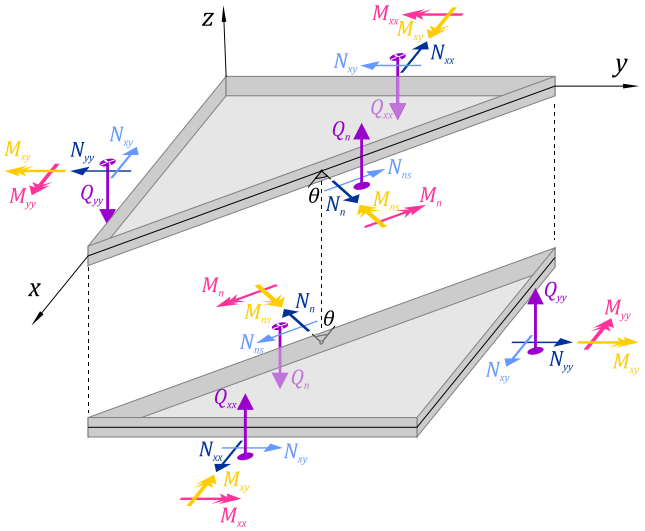

Fig. 3 Force and moment resultants on a plate element (Reddy 2004)

$$\begin{aligned}0=&\int_{\Omega^e}\left[\frac{\partial\delta u}{\partial x}N_{xx}+\frac{\partial\delta u}{\partial y}N_{xy}\right]dxdy-\int_{\Gamma^e}\delta uN_n ds\\ 0=&\int_{\Omega^e}\left[\frac{\partial\delta v}{\partial x}N_{xy}+\frac{\partial\delta v}{\partial y}N_{yy}\right]dxdy-\int_{\Gamma^e}N_{ns}\delta v ds\\ 0=&-\int_{\Omega^e}\left[\frac{\partial^2\delta w}{\partial x^2}M_{xx}+2\frac{\partial^2\delta w}{\partial x\partial y}M_{xy}+\frac{\partial^2\delta w}{\partial y^2}M_{yy}\right.\\ &\left.+\delta wq\right]dxdy\\ &-\int_{\Gamma^e}\left[\delta wV_n+\frac{\partial\delta w}{\partial n}M_n\right]ds\end{aligned} \tag{7}$$

2.4.2 Interpolation and finite element model

Approximations of the displacements (u,v,w) are carried out by interpolations of the form,

$$\begin{aligned}u=\sum_{j=1}^{n}u_j\psi_j(x,y)\quad,\quad v=\sum_{j=1}^{n}v_j\psi_j(x,y)\quad,\\ w=\sum_{j=1}^{m}\Delta_j\varphi_j(x,y)\end{aligned} \tag{8}$$

where (u_j,v_j) and Δ_j correspond to the nodal values of (u,v) and w and its derivatives. $\left(\psi_j,\varphi_j\right)$ are the Lagrange and Hermite interpolation functions, respectively (Baltacı *et al.* 2006, Ochoa and Reddy 1992).

By substituting the displacements approximations (Eq. (8)) for (u,v,w), and $\delta u=\psi_i$, $\delta v=\psi_i$ and $\delta w=\phi_i$ into the obtained weak forms in Eq. (7) the finite element models of equilibrium equations of classical laminated plate theory for static case Eq. (5) are reached

$$0 = \int_{\Omega^e} \left[\frac{\partial \psi_i}{\partial x} N_{xx} + \frac{\partial \psi_i}{\partial y} N_{xy}\right] dxdy - \int_{\Gamma^e} N_n \psi_i ds$$

$$0 = \int_{\Omega^e} \left[\frac{\partial \psi_i}{\partial x} N_{xy} + \frac{\partial \psi_i}{\partial y} N_{yy}\right] dxdy - \int_{\Gamma^e} N_{ns} \psi_i ds$$

$$0 = -\int_{\Omega^e} \left[\frac{\partial^2 \phi_i}{\partial x^2} M_{xx} + 2\frac{\partial^2 \phi_i}{\partial x \partial y} M_{xy} + \frac{\partial^2 \phi_i}{\partial y^2} M_{yy} + \phi_i q\right] dxdy - \int_{\Gamma^e} \left[\phi_i V_n + \frac{\partial \phi_i}{\partial n} M_n\right] ds \quad (9)$$

These equations can be expressed by the form,

$$[\boldsymbol{K^e}]\{\boldsymbol{\Delta^e}\} - \{\boldsymbol{F^e}\} = \{\boldsymbol{0}\} \quad (10)$$

where $\boldsymbol{K^e}$ is the stiffness matrix and $\boldsymbol{F^e}$ is the force vector.

For buckling analysis the expression Eq. (10) takes the form,

$$([\boldsymbol{K^e}] - \lambda \cdot [\boldsymbol{S^e}])\{\boldsymbol{\Delta_o^e}\} = \{\boldsymbol{F_o^e}\} \quad (11)$$

where $[\boldsymbol{S^e}]$ is the stability matrix and the eigenvalue λ represents the ratio of actual buckling load to the applied in-plane forces:

$$\lambda = \frac{N_{xx}}{\bar{N}_{xx}} = \frac{N_{yy}}{\bar{N}_{yy}} = \frac{N_{xy}}{\bar{N}_{xy}} \quad (12)$$

where $(\bar{N}_{xx}, \bar{N}_{yy}, \bar{N}_{xy})$ are applied in-plane forces (Fig. 4) (Ochoa and Reddy 1992).

2.5 Plate stability

The energy method is more efficient than the equilibrium method while detecting the critical buckling loads of the plates with complex geometry and mixed boundary conditions.

The neutral equilibrium state takes place when the variation of the total potential is equal to zero ($\Delta\Pi = 0$). By employing this energy criterion, the critical buckling load analysis of plates can be performed. The variation of the total potential energy increment of a plate subjected to in-plane loading is given by

$$\Delta\Pi = \Pi - \Pi_0 = \Delta U_0 + U_b + \Delta\Omega_\Gamma \quad (13)$$

Herein, ΔU_0 represents the strain energy gain of the plate middle surface due to buckling; U_b denotes the bending and twisting part of the strain energy and $\Delta\Omega_\Gamma$ stands for the potential increment of the in-plane external forces (Ventsel and Krauthammer 2001, Szilard 2004)

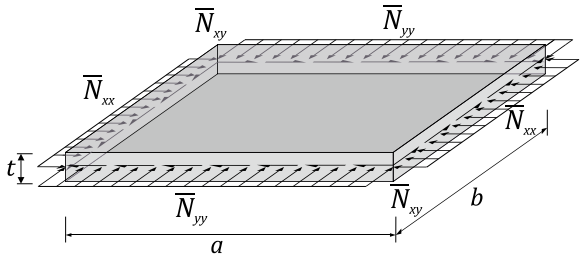

Fig. 4 A rectangular plate element with applied in-plane compressive and shear forces

$$\Delta U_0 = \iint_A \left(N_{xx}.\varepsilon_{xx} + N_{yy}.\varepsilon_{yy} + N_{xy}.\varepsilon_{xy}\right) dA \quad (14)$$

$$\varepsilon_{xx} = \frac{\partial u}{\partial x} + \frac{1}{2}\left(\frac{\partial w}{\partial x}\right)^2$$
$$\varepsilon_{yy} = \frac{\partial v}{\partial y} + \frac{1}{2}\left(\frac{\partial w}{\partial y}\right)^2 \quad (15)$$
$$\varepsilon_{xy} = \frac{\partial u}{\partial y} + \frac{\partial v}{\partial x} + \frac{\partial w}{\partial x}\frac{\partial w}{\partial y}$$

Substituting Eq. (15) into Eq. (14) yields Eq. (16) for the strain energy gain of the plate middle surface

$$\Delta U_0 = \iint_A \left[N_{xx}\frac{\partial u}{\partial x} + N_{yy}\frac{\partial v}{\partial y} + N_{xy}\left(\frac{\partial u}{\partial y} + \frac{\partial v}{\partial x}\right)\right] dA + \frac{1}{2}\iint_A \left[N_{xx}\left(\frac{\partial w}{\partial x}\right)^2 + N_{yy}\left(\frac{\partial w}{\partial y}\right)^2 + 2N_{xy}\left(\frac{\partial w}{\partial x}\frac{\partial w}{\partial y}\right)\right] dA \quad (16)$$

The work of the in-plane external forces is denoted as W_e. Thus, Eq. (16) can be put the form

$$\Delta U_0 = W_e + \frac{1}{2}\iint_A \left[N_{xx}\left(\frac{\partial w}{\partial x}\right)^2 + N_{yy}\left(\frac{\partial w}{\partial y}\right)^2 + 2N_{xy}\left(\frac{\partial w}{\partial x}\frac{\partial w}{\partial y}\right)\right] dA \quad (17)$$

The potential variation of the in-plane external forces is equal to the negative value of the work done by these forces

$$\Delta\Omega_\Gamma = -W_e \quad (18)$$

Also the bending and twisting part of the strain energy, U_b, is given by

$$U_b = \frac{1}{2}\iint_A D\left\{\left(\frac{\partial^2 w}{\partial x^2} + \frac{\partial^2 w}{\partial y^2}\right)^2 - 2(1-\nu)\left[\frac{\partial^2 w}{\partial x^2}\frac{\partial^2 w}{\partial y^2} - \left(\frac{\partial^2 w}{\partial x \partial y}\right)^2\right]\right\} dA \quad (19)$$

Therefore, the variation of the total potential energy of the plate upon buckling, $\Delta\Pi$, can be obtained by assembling equivalents of ΔU_0, U_b and $\Delta\Omega_\Gamma$ expressions in Eq. (13) as below (Ventsel and Krauthammer 2001, Szilard 2004)

$$\Delta\Pi = \left(W_e + \frac{1}{2}\iint_A \left[N_{xx}\left(\frac{\partial w}{\partial x}\right)^2 + N_{yy}\left(\frac{\partial w}{\partial y}\right)^2 + 2N_{xy}\left(\frac{\partial w}{\partial x}\frac{\partial w}{\partial y}\right)\right] dA\right) + \left(\frac{1}{2}\iint_A D\left\{\left(\frac{\partial^2 w}{\partial x^2} + \frac{\partial^2 w}{\partial y^2}\right)^2\right.\right.$$

$$-2(1-\nu)\left[\frac{\partial^2 w}{\partial x^2}\frac{\partial^2 w}{\partial y^2}-\left(\frac{\partial^2 w}{\partial x \partial y}\right)^2\right]\Bigg\}dA\Bigg) \quad (20)$$
$$+(-W_e)$$

$$\Delta\Pi = \frac{1}{2}\iint_A \left[N_{xx}\left(\frac{\partial w}{\partial x}\right)^2 + N_{yy}\left(\frac{\partial w}{\partial y}\right)^2 + 2N_{xy}\left(\frac{\partial w}{\partial x}\frac{\partial w}{\partial y}\right)\right]dA$$
$$+\frac{1}{2}\iint_A D\left\{\left(\frac{\partial^2 w}{\partial x^2}+\frac{\partial^2 w}{\partial y^2}\right)^2 \right. \quad (21)$$
$$\left. -2(1-\nu)\left[\frac{\partial^2 w}{\partial x^2}\frac{\partial^2 w}{\partial y^2}-\left(\frac{\partial^2 w}{\partial x \partial y}\right)^2\right]\right\}dA$$

3. Present study

In present work, a numerical study by using ANSYS Mechanical software based on finite element method was carried out. In the analysis, the plate elements were assumed to be laminated composite plates and, variation of linear/curvilinear free-edge forms, various cutout shapes with/out rounded corner and diverse lamination configurations were used as design parameters. Within this scope, 14 types of lamination configuration were specified according to various orientation angles, number and thickness of plies. In addition, 6 different types of cutout and 3 different shapes of free-edge form were determined. By combining all of these, 294 different critical buckling load analyses were performed.

Therefore, the variation of the total potential energy of the plate upon buckling, ΔΠ, can be obtained by assembling equivalents of ΔU_0, U_b and $\Delta\Omega_\Gamma$ expressions in Eq. (13) as below (Ventsel and Krauthammer 2001, Szilard 2004)

3.1 Materials

The considered laminates were constructed of carbon/epoxy with material properties in Table 1. Dimensions of the designed laminated plates from a corner to its neighbor one were equal and 1 m for all diverse forms. Plates were simply supported on the edges parallel to y-axis and also under in-plane compressive loading in x-direction on these edges. On the other hand, the edges parallel to x-axis were free and have three different forms

Table 1Material properties of carbon/epoxy (ANSYS 2014)

Elasticity Modulus [GPa]	
E_1	$E_2 = E_3$
121,0	8,6
Shear Modulus [GPa]	
$G_{12} = G_{13}$	G_{23}
4,7	3,1
Poisson Ratios	
$\upsilon_{12} = \upsilon_{13}$	υ_{23}
0,27	0,40

according to the type of the plate. The 3 types of plates, namely linear, convex curvilinear and concave curvilinear edged were schematized as "[ ]", "( )" and ")(", respectively. In Fig. 5, the difference between the free-edges forms and the details of boundary conditions are illustrated.

6 different cutout shapes, with/out rounded corner, located in the middle of the plate were determined and, labeling and dimensions of cutouts are specified as presented in Fig. 6.

The ply thicknesses of the laminates vary depending on the number of ply included in each laminate and the total thickness was 36 mm for all laminates. The details of the determined lamination configurations and all combinations of plate form and cutout shape parameters are presented in Fig. 7. By using the all defined parameters, totally 294 different case combinations were generated.

3.2 Methods

The critical buckling loads of the depicted laminated plates were predicted by using the Linear Buckling Analysis in ANSYS Mechanical software. Preliminarily the all combinations of the plate type and the cutout shape designs were geometrically modeled. Then orthotropic lamination specifications were defined for each combination separately.

Thereafter, the meshing processes were realized. In analysis, four nodded SHELL181 elements with six degrees of freedom at each node, which is suitable for thin to moderately-thick shell structures, were used to model the

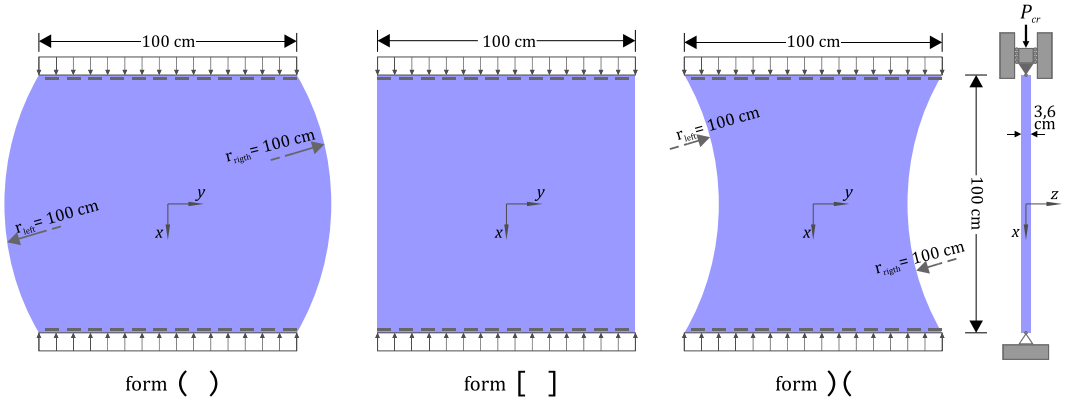

Fig. 5 Dimensions, boundary conditions and free-edges forms of plate types

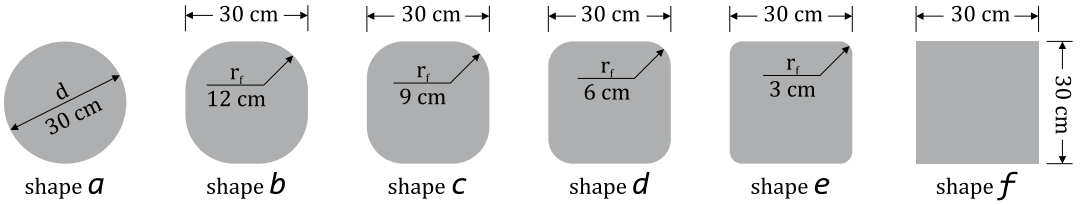

Fig. 6 Dimensions and labels of cutout shapes

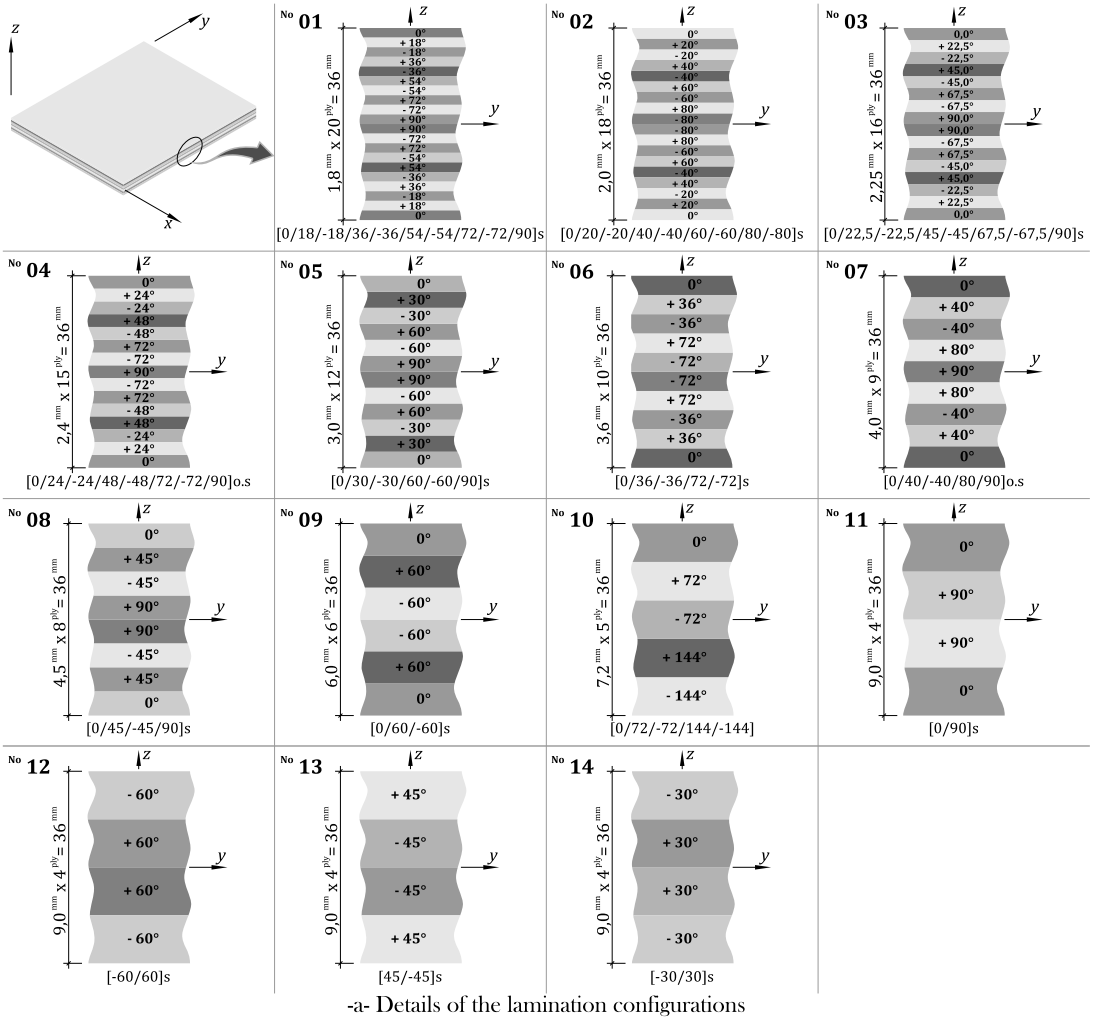

-a- Details of the lamination configurations

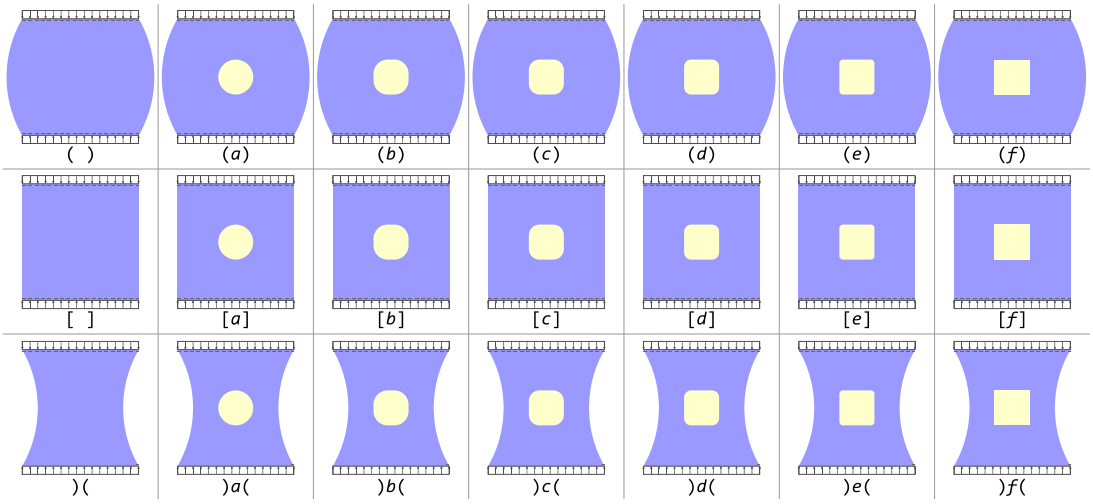

-b- Combinations of plate form and cutout shape parameters

Fig. 7 All defined parameters and combinations

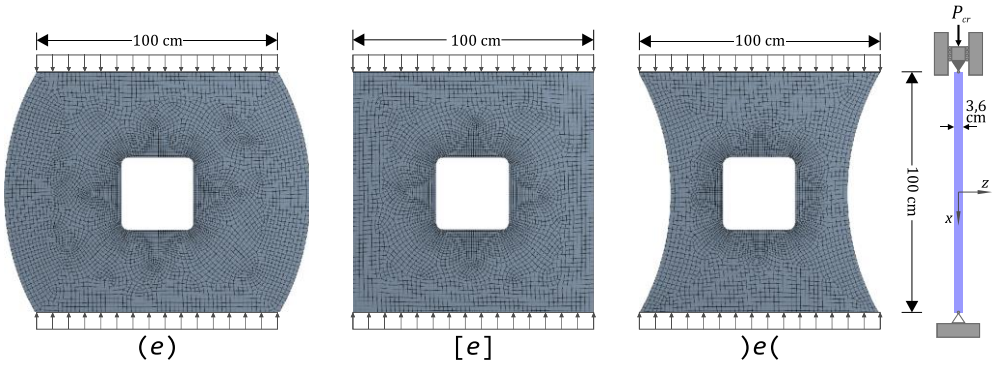

Fig. 8 Typical finite element mesh structures and boundary conditions of the models with cutout "*e*" shape

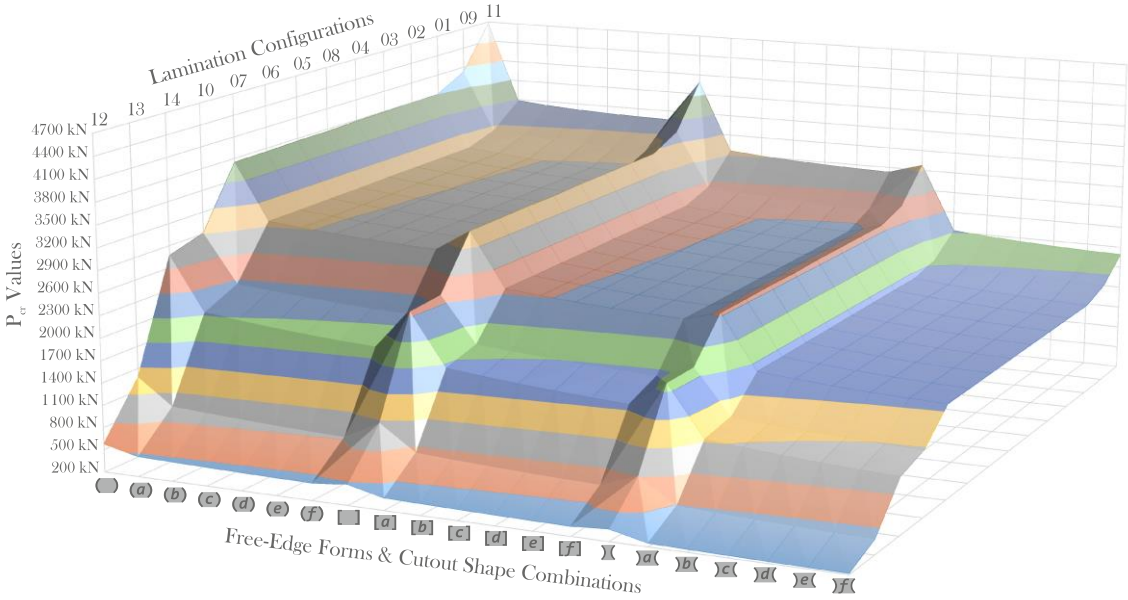

Fig. 9 3D-surface chart of the P_{cr} values for all the combinations of the parameters

laminated plates. In consequence of different plate forms and various cutout shapes, several models and mesh structures were generated. Fig. 8 illustrates the typical finite element mesh structures and boundary conditions of the models. The element sizes of mesh structures here were adjusted as halved thickness size of laminate. Later on, as can be seen in Fig. 8, one and a half times smaller meshes than the others were arranged in the region of the cutout edges where stress concentrations were expected.

Sequentially, the simply supported boundary condition was applied on one of the edges parallel to *y* axis by fixing the translational displacements in all directions and, the sliding supported boundary condition was assigned to the opposite edge of the one by only releasing the translational displacement in *x* axis. Then this edge was subjected to the compression load uniformly. Herein, unit load value of linear buckling analysis was determined as 1 [N/m]. Ultimately, solving processes were started and obtained results were collected.

4. Results and discussions

The all obtained critical buckling load results (P_{cr}) from the analyses are represented by a 3D-surface graphic in Fig. 9. To have the opportunity to carry out an accurate evaluation of the results, one is discussed in three subheadings according to the effects of lamination configurations, free-edge forms and cutout shapes.

4.1 Effects of lamination configurations

This section deals with the effects of the lamination configurations on the critical buckling load (P_{cr}) values. If we evaluate the changes in P_{cr} values with regard to the lamination configurations by Table 2, Fig. 9 and Fig. 10, the following assessments could be made;

- Although the proportional alterations of bending stiffness values of lamination configurations may seem somewhat different, a good agreement with the proportional changes of critical buckling load values (Table 2).
- The P_{cr} values of *no.11* lamination has the highest values for each combination of the plate forms and the cutout shapes (Fig. 9 & Fig. 10). Withal the bending stiffness of *no.11* lamination is the maximal among the others (Table 2).
- In contrast with *no.11* lamination, the proportional

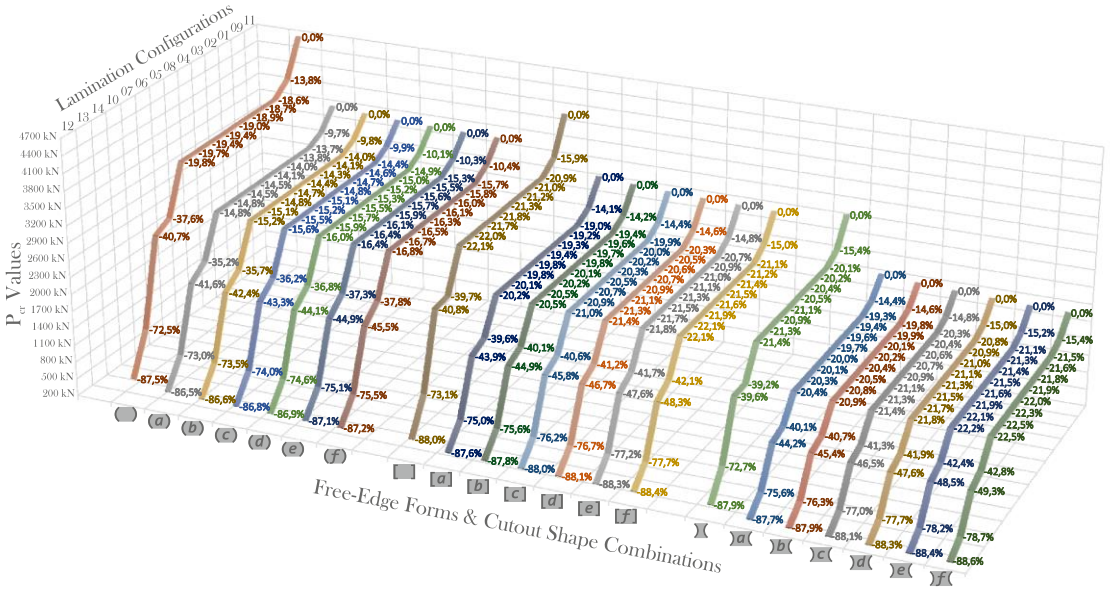

Fig. 10 3D-line chart of the P_{cr} values and relative changes depending on the lamination configurations

Table 2 Values of bending stiffness (D_{11}) and normalized alterations of them with respect to the highest one of lamination configurations (Sorted in descending order by values)

	Lamination Configuration	*Bending Stiffness* [N.mm]	*Decline* [%]
no.11	[0/90]s	107267,7	0,0 %
no.9	[0/60/-60]s	88102,9	17,9 %
no.8	[0/45/-45/90]s	78012,0	27,3 %
no.1	[0/18/-18/36/-36/54/-54/72/-72/90]s	77794,1	27,5 %
no.2	[0/20/-20/40/-40/60/-60/80/-80]s	77641,7	27,6 %
no.3	[0/22,5/-22,5/45/-45/67,5/-67,5/90]s	77450,2	27,8 %
no.4	[0/24/-24/48/-48/72/-72/90]o.s	77353,5	27,9 %
no.5	[0/30/-30/60/-60/90]s	76972,5	28,2 %
no.7	[0/40/-40/80/90]o.s	76919,3	28,3 %
no.6	[0/36/-36/72/-72]s	76896,0	28,3 %
no.10	[0/72/-72/144/-144]	66856,7	37,7 %
no.14	[-30/30]s	33209,6	69,0 %
no.13	[45/-45]s	15140,3	85,9 %
no.12	[-60/60]s	9908,9	90,8 %

difference of *no.12* lamination exhibits averagely about *88%* decline and also has the lowest values for each combination (Fig. 9 and Fig. 10). Besides, for *no.12* lamination the decreases in the P_{cr} values between the cases with/out cutouts plot far less steep graphs than the others in Fig. 12.

• Between *no.1,2,3,4,5,6,7,8* laminations and *no.11*, which performs the maximum P_{cr} values, the proportional differences are averagely *about 19,0%* and also plots of these 8 laminations are almost overlapping (Fig. 11 and Fig. 12). Similarly, the bending stiffness values of these are adjacent each other.

• The P_{cr} and the bending stiffness values of *no.9* lamination is separated with a minor difference from the gathering region of *no.1,2,3,4,5,6,7,8* in Table 2, Fig. 11 and Fig. 12.

• The distinct proximity of the P_{cr} values of *no.1,2,3,4,5,6,7,8* laminations could be associated with the lamination orientation of outmost plies within 10 [mm] depth which vary between 0° and 45°. Thereby, it presents the efficiency of gathering the plies oriented by *under 45° at* the outmost of the laminates on the P_{cr} values.

• The proportional differences of the P_{cr} values between the highest valued *no.11* lamination and the lowest valued *no.12* lamination are averagely about *88%* decline (Fig. 10). As the orientation angels approach zero at the outmost plies, the bending stiffness and by extension critical buckling load are increase (Table 2). It shows significance of the orientation angels on the critical buckling loads (P_{cr}) even both laminations consisting of symmetric four layered structure and have only difference in orientation angels.

4.2 Effects of free-edge forms

In this section, the effects of linear and curvilinear free-edge forms are examined on the P_{cr} values. As mentioned earlier, three different free-edge forms were determined, namely convex curvilinear "( )", linear "[ ]" and concave curvilinear ") (" edged. The geometric details of these edge forms in Fig. 5 indicate that between the "[ ]" and either "( )", or ") (" edged forms same amount of material was increased or decreased, respectively. The alterations in the P_{cr} values with respect to the free-edge forms are presented in Table 3 and Fig. 11. According to the outcomes, the following assessments could be derived as remarkable points;

• The differences of the P_{cr} values between linear "[ ]" and concave curvilinear ") (" edged forms are greater than the ones between linear " [ ] " and convex curvilinear "( )"edged forms (Table 3 and Fig. 11).

• In the proportional differences in respect of the P_{cr} values of the linear "[ ]" edged forms, the averages of

Table 3 The proportional P_{cr} values depending on the free-edge forms with gradually highlighted values in respect of the lamination configurations in each. (The darker-red and -blue highlights are max. and min. extremums of absolute values, respectively.)

Lamination Configurations	( ) « [ ] »)(		(a) « [a] »)a(		(b) « [b] »)b(		(c) « [c] »)c(		(d) « [d] »)d(		(e) « [e] »)e(		(f) « [f] »)f(	
12	21,9%	-24,4%	28,7%	-32,0%	29,4%	-32,7%	30,0%	-33,3%	30,5%	-33,8%	30,9%	-34,1%	31,3%	-34,2%
13	20,0%	-24,1%	27,3%	-33,2%	28,1%	-34,1%	28,9%	-34,9%	29,4%	-35,5%	29,9%	-35,9%	30,5%	-36,2%
14	17,4%	-23,8%	22,7%	-31,9%	23,4%	-32,7%	23,8%	-33,3%	24,3%	-33,9%	24,7%	-34,3%	25,3%	-34,5%
10	21,3%	-24,8%	26,2%	-32,1%	26,6%	-32,7%	27,0%	-33,2%	27,2%	-33,6%	27,5%	-33,9%	27,8%	-34,0%
07	20,8%	-24,7%	25,6%	-31,8%	26,0%	-32,3%	26,3%	-32,8%	26,6%	-33,1%	26,9%	-33,4%	27,1%	-33,5%
06	20,7%	-24,7%	25,5%	-31,8%	25,9%	-32,3%	26,3%	-32,8%	26,6%	-33,1%	26,8%	-33,4%	27,1%	-33,5%
05	20,7%	-24,6%	25,5%	-31,8%	25,9%	-32,3%	26,3%	-32,8%	26,6%	-33,1%	26,8%	-33,4%	27,1%	-33,6%
08	20,8%	-24,7%	25,5%	-31,8%	25,9%	-32,3%	26,2%	-32,8%	26,5%	-33,1%	26,8%	-33,4%	27,0%	-33,5%
04	20,6%	-24,6%	25,5%	-31,8%	25,9%	-32,3%	26,3%	-32,8%	26,6%	-33,1%	26,8%	-33,4%	27,0%	-33,6%
03	20,6%	-24,6%	25,5%	-31,8%	25,9%	-32,3%	26,3%	-32,8%	26,6%	-33,1%	26,8%	-33,4%	27,0%	-33,6%
02	20,6%	-24,6%	25,5%	-31,8%	25,9%	-32,3%	26,3%	-32,8%	26,6%	-33,1%	26,8%	-33,4%	27,0%	-33,6%
01	20,6%	-24,6%	25,5%	-31,8%	25,9%	-32,3%	26,3%	-32,8%	26,6%	-33,1%	26,8%	-33,4%	27,0%	-33,6%
09	20,2%	-24,9%	23,7%	-31,8%	24,1%	-32,3%	24,4%	-32,8%	24,7%	-33,1%	25,0%	-33,4%	25,2%	-33,5%
11	17,2%	-25,4%	17,7%	-31,6%	18,0%	-32,1%	18,2%	-32,5%	18,4%	-32,8%	18,7%	-33,1%	18,9%	-33,2%

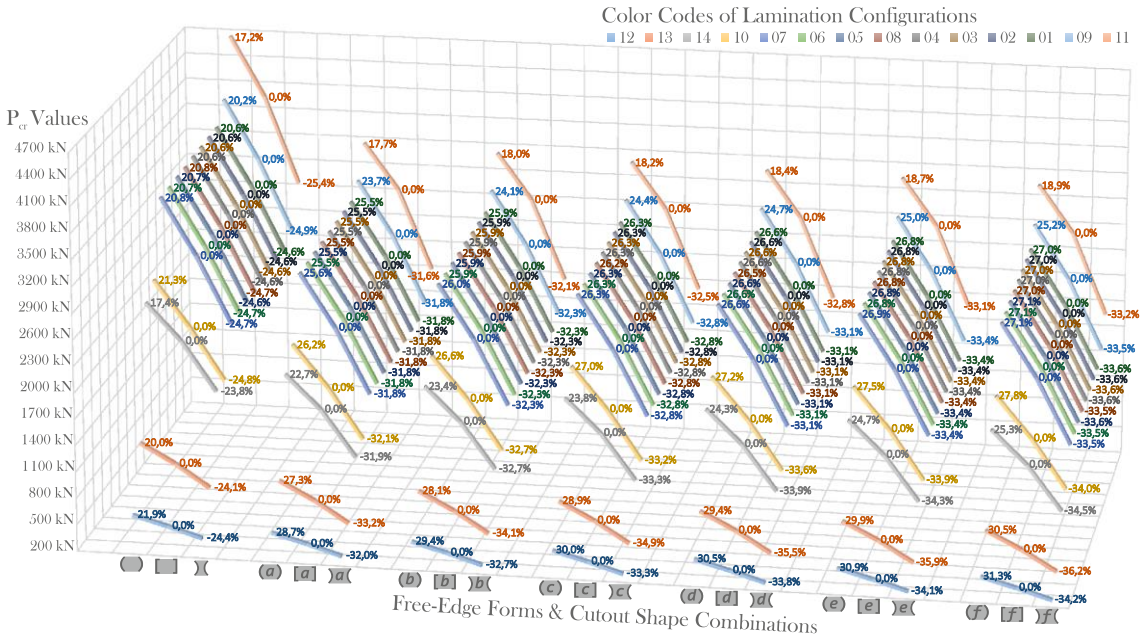

Fig. 11 3D-line chart of the P_{cr} values and relative changes depending on the free-edge forms

the alterations to "( )" and to ") (" from "[ ]" edged forms are around 20,3% and -24,6% for the cases without cutout, respectively; as well for the cases with cutout the averages of the ones are around 26,3% and -33,1%, respectively (Table 3 and Fig. 11).

• Concerning *no.1,2,3,4,5,6,7,8* laminations, between "[ ]" and "( )" edged forms and between "[ ]" and ") (" edged forms the proportional differences are averagely around;

20,7% and -24,7% as for the cases without cutout,
25,5% and -31,8% as for the cases with cutout "*a*",
25,9% and -32,3% as for the cases with cutout "*b*",
26,3% and -32,8% as for the cases with cutout "*c*",
26,6% and -33,1% as for the cases with cutout "*d*",
26,8% and -33,4% as for the cases with cutout "*e*",
27,0% and -33,6% as for the cases with cutout "*f*",

respectively (Table 3 and Fig. 11).

• Concerning *no.14* lamination, between "( )" and ") (" edged forms the proportional difference declines around -41,2% which is the lowest alteration among the all laminations (Table 3 and Fig. 11).

• For the cases without cutout, the absolute total proportional changes of the P_{cr} values between "( )"and ") (" edged forms considering the ones of the linear "[ ]" edged forms have the lowest alteration for *no.14* lamination by around 41,2% (Table 3 and Fig. 11). It demonstrates that when angels between load direction and the orientation directions get close to 0°, the effectiveness of the width change by free-edge form parameter diminish.

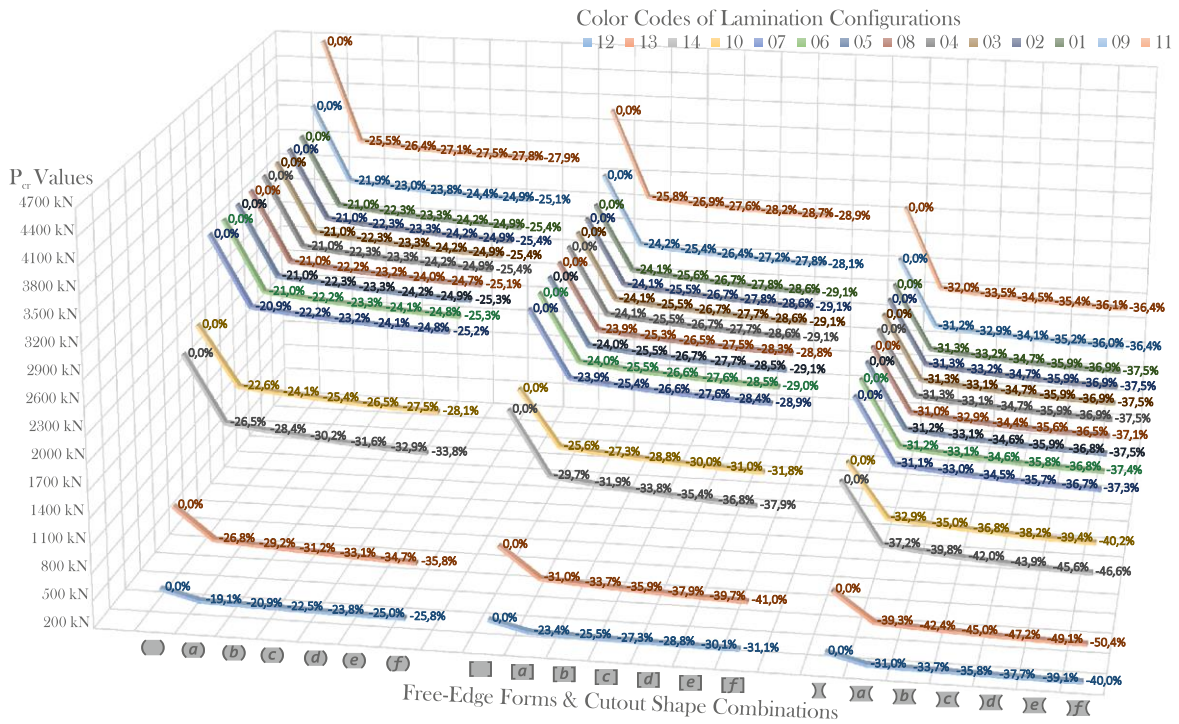

Fig. 12 3D-line chart of the P_{cr} values and relative changes depending on the cutout shapes

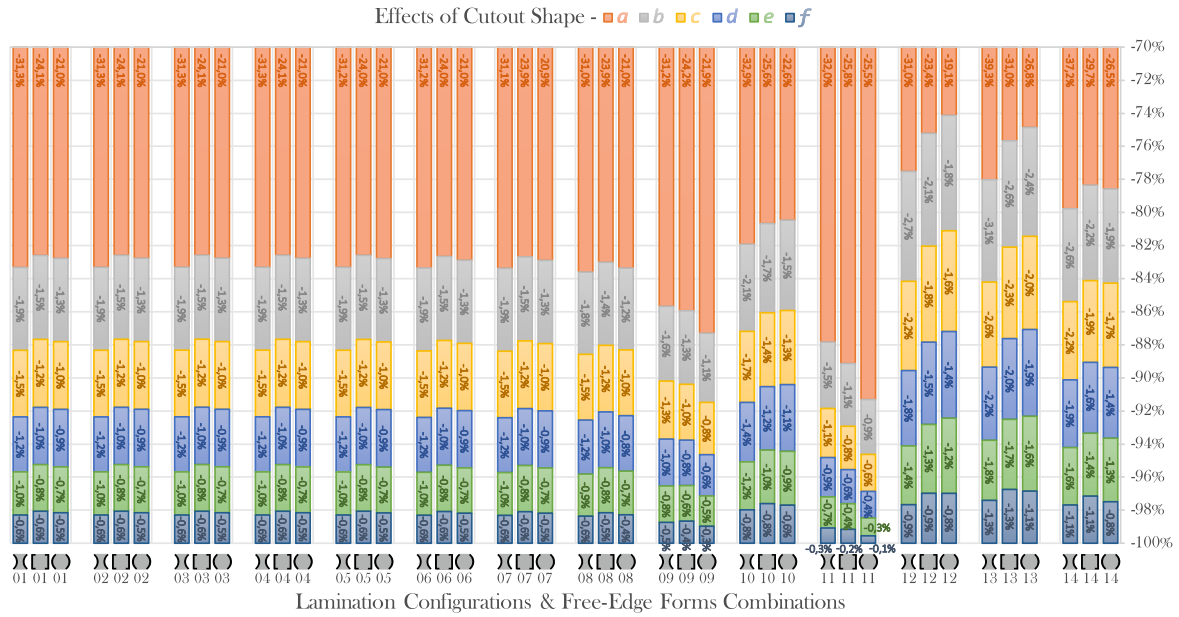

Fig. 13 Percentage distribution of the proportional P_{cr} alterations depending on the cutout shapes

4.3 Effects of cutout shapes

This section deals with the effects of the various cutout shapes with/out rounded corner on the critical buckling loads (Fig. 12 and Fig. 13).

• For each free-edge form, the P_{cr} values with respect to the cutout shapes are explicitly different from each other, nevertheless the changing trends and slopes are quite similar (Fig. 12).

• Concerning *no.1,2,3,4,5,6,7,8* laminations, in the proportional differences with respect to the P_{cr} values of the cases without cutout, the alterations depending on the cutout shapes (from shape "*a*" to "*f*") averagely decline in the interval between;

-21,0% and -25,4% as for the cases with "( )"
-24,0% and -29,0% as for the cases with "[ ]"
-31,0% and -37,5% as for the cases with ") ("

edged forms. And also, the plots of these 8 laminations are almost overlapping for each (Fig. 12).

• Concerning *no.11* lamination, the variation between the highest and the lowest proportional differences is around;

2,5% as for the cases with "( )"
3,1% as for the cases with "[ ]"

4,4% as for the cases with “) (“
edged forms which are the lowest alterations for each (Fig. 12).

• Concerning *no.13* lamination, the proportional differences decline in the interval between;
-26,8% and -35,8% as for the cases with “( )”
-31,0% and -41,0% as for the cases with “[ ]”
-39,3% and -50,4% as for the cases with “) (“
edged forms which represent the highest reduction amounts for each, depending on the cutout shapes (from shape “a” to “f”). And also the differences between bounds of these intervals give the highest changes of the ones for each form by;
9,0% as for the cases with “( )”
10,0% as for the cases with “[ ]”
11,1% as for the cases with “) (“
edged forms (Fig. 12).

• Concerning *no.12* lamination with (a), (b), (c) and (d) cutout and edge forms, the proportional differences decline in the interval between -19,1% and -23,8% which represent the lowest reduction amounts (Fig. 12). Besides, the one with $[a]$ cutout and edge form, the proportional difference declines by -23,4% which is the lowest change (Fig. 12).

5. Conclusions

In the present study, the critical buckling loads (P_{cr}) of the generated plate combinations by lamination configuration, cutout shape and free-edge form parameters were analyzed by ANSYS finite element software. Following points were reached from the results obtained here.

• The alterations depending on the lamination configurations are sharper than those based on the cutout shape and the free-edge form parameters. Hence, it shows that even having same material properties and fixed total thickness, the lamination configuration exhibited significant effect on the critical buckling load (P_{cr}) values. Which indicates that there are substantial relations between bending stiffness and critical buckling load.

• The average proportional P_{cr} value variations between from “[ ]” edged form to “( )” and to “) (“show that the alteration ratios are not equal as the amount of material change of plates are. Besides, the effect levels of the free-edge forms on the P_{cr} values significantly depending on lamination configurations.

• The proportional alterations of the P_{cr} values according to the cutout shapes are primarily depending on lamination configurations. Also, the proportional alterations in each interval between cutout shapes are nearly equal.

In summary, the main conclusion to be drawn from this study could be that the critical buckling load (P_{cr}) values of laminated composite plates are apparently influenced by lamination configurations and cutout existence by up to 88% capacity loss. The effects of free-edge form and cutout shape parameters are more limited than the other, comparatively.

It may be suggested that the following alternative conditions, forms and methods could be carried out in future;

• Existence of delamination defects,
• Considering the mid-surface form as non-flat,
• Evaluating by non-linear analysis methods,
• Including local stiffeners,
• In-plane compression effect on cutout edges.

References

Al-Jameel, S.E.S. and Albazzaz, R.K. (2014), “Buckling analysis of composite plate with central elliptical cut out”, *Al-Rafidain Eng. J.*, **22**(1), 14-25.

Al-Qablan, H., Dwairi, H., Shatarat, N., Rosan, T. and Al-Qablan, T. (2010), “Stability analysis of composite panels with stiffeners and circular cutouts”, *Jordan J. Civil Eng.*, **4**(2), 119-131.

Al-Qablan, H., Katkhuda, H. and Dwairi, H. (2009), “Assessment of the buckling behavior of square composite plates with circular cutout subjected to in-plane shear”, *Jordan J. Civil Eng.*, **3**(2), 184-195.

ANSYS® Mechanical, Release 14.

Baba, B.O. (2007), “Buckling behavior of laminated composite plates”, *J. Reinf. Plast. Compos.*, **26**(16), 1637-1655.

Baba, B.O. and Baltaci, A. (2007), “Buckling characteristics of symmetrically and antisymmetrically laminated composite plates with central cutout”, *Appl. Compos. Mater.*, **14**(4), 265-276.

Baltaci, A., Sarikanat, M. and Yildiz, H. (2007), “Static stability of laminated composite circular plates with holes using shear deformation theory”, *Finite Elem. Anal. Des.*, **43**(11-12), 839-846.

Baltacı, A., Sarıkanat, M. and Yıldız, H. (2006), “Buckling analysis of laminated composite circular plates with holes”, *J. Reinf. Plast. Compos.*, **25**(7), 733-744.

Carpinteri, A., Bazzucchi, F. and Manuello, A. (2016), “Nonlinear instability analysis of long-span roofing structures: The case-study of Porta Susa railway-station”, *Eng. Struct.*, **110**48-58.

Civalek, O. (2008), “Free vibration analysis of symmetrically laminated composite plates with first-order shear deformation theory (FSDT) by discrete singular convolution method”, *Finite Elem. Anal. Des.*, **44**(12-13), 725-731.

Civalek, O. (2009), “Fundamental frequency of isotropic and orthotropic rectangular plates with linearly varying thickness by discrete singular convolution method”, *Appl. Math. Model.*, **33**(10), 3825-3835.

Ghannadpour, S., Najafi, A. and Mohammadi, B. (2006), “On the buckling behavior of cross-ply laminated composite plates due to circular/elliptical cutouts”, *Compos. Struct.*, **75**(1), 3-6.

Guo, S., Zhou, L. and Cheung, C. (2008), “Cutout reinforcements for shear loaded laminate and sandwich composite panels”, *Int. J. Mech. Mater. Des.*, **4**(2), 157-171.

Islam, S.M.Z., Abang-Abdullah, A.A. and Jafar, M.S. (2005), “Finite element and experimental investigation on profiled steel sheet to develop self-supporting roofing element”, *J. Appl. Sci.*, **5**(6), 1113-1121.

Jadhav, S.S. and Chavan, D.S. (2013), “Fem & experimental analysis of composite laminate with elliptical cut out using reflection polariscope”, *Int. J. Adv. Eng. Tech/IV/III*, **67**, 71, July-September.

Joshi, A., Reddy, P.R., Krishnareddy, V.N. and Sushma, C.V. (2013), “Buckling analysis of thin carbon/epoxy plate with circular cut-outs under biaxial compression by using fea”, *Int. J. Res. Eng. Tech.*, **2**(10), 296-301.

Kumar, D. and Singh, S.B. (2010), "Effects of boundary conditions on buckling and postbuckling responses of composite laminate with various shaped cutouts", *Compos. Struct.*, **92**(3), 769-779.

Narayana, A.L., Rao, K. and Kumar, R.V. (2014), "Buckling analysis of rectangular composite plates with rectangular cutout subjected to linearly varying in-plane loading using fem", *Sadhana*, **39**(3), 583-596.

Nebelsick, J. and Halbe, R. (2014), http://www.archdaily.com/520897/landesgartenschau-xhibition-hall-icd-itke-iigs-university-of-tuttgart/Landesgartenschau Exhibition Hall / ICD/ITKE/IIGS University of Stuttgart.

Ochoa, O.O. and Reddy, J.N. (1992), *Finite Element Analysis of Composite Laminates*, Kluwer Academic Publishers, Netherland.

Ö zben, T. (2009), "Analysis of critical buckling load of laminated composites plate with different boundary conditions using fem and analytical methods", *Comput. Mater. Sci.*, **45**(4), 1006-1015.

Reddy, J.N. (2004), *Mechanics of Laminated Composite Plates and Shells: Theory and Analysis*, 2nd Edition, CRC Press, Washington.

Reddy, J.N., Arciniega, R.A. and Moleiro, F. (2010), "Finite element analysis of composite plates and shells", *Encyclopedia of Aerospace Engineering*.

Rezaiee-Pajand, M., Shahabian, F. and Tavakoli, F.H. (2012), "A new higher-order triangular plate bending element for the analysis of laminated composite and sandwich plates", *Struct. Eng. Mech.*, **43**(2), 253-271.

Shukla, K., Nath, Y., Kreuzer, E. and Kumar, K. (2005), "Buckling of laminated composite rectangular plates", *J. Aerosp. Eng.*, **18**(4), 215-223.

Singh, S.K. and Chakrabarti, A. (2012), "Buckling analysis of laminated composite plates using an efficient c0 fe model", *Latin Am. J. Solid. Struct.*, **9**(3), 1-13.

Szilard, R. (2004), *Theories and Applications of Plate Analysis: Classical, Numerical, and Engineering Methods*, John Wiley & Sons, Hoboken, N.J.

Thai, H.T. and Choi, D.H. (2014), "Finite element formulation of a refined plate theory for laminated composite plates", *J. Compos. Mater.*, **48**(28), 3521-3538.

Ventsel, E. and Krauthammer, T. (2001), *Thin Plates and Shells: Theory, Analysis, and Applications*, Marcel Dekker, New York.

Yazdani, S., Rahimi, G. and Ghanbari, M. (2013), "Experimental and numerical stress analysis of fml plates with cutouts under in-plane loading", *Mech.*, **19**(2), 128-134.

Yazici, M. (2009), "Influence of cut-out variables on buckling behavior of composite plates", *J. Reinf. Plast. Compos.*, **28**(19), 2325-2339.

Yazici, M., Ozcan, R., Ulku, S. and Okur, I. (2003), "Buckling of composite plates with u-shaped cutouts", *J. Compos. Mater.*, **37**(24), 2179-2195.

Zerin, Z., Turan, F. and Başoğlu, M.F. (2016), "Examination of non-homogeneity and lamination scheme effects on deflections and stresses of laminated composite plates", *Struct. Eng. Mech.*, **57**(4), 603-616.

Zhong, H. and Gu, C. (2007), "Buckling of symmetrical cross-ply composite rectangular plates under a linearly varying in-plane load", *Compos. Struct.*, **80**(1), 42-48.